

**UCSF**

**UC San Francisco Electronic Theses and Dissertations**

**Title**

Improving Pyruvate Kinetic Measurements Using Variable Flip Angle Schemes in bSSFP Hyperpolarized Carbon-13 MR Imaging

**Permalink**

<https://escholarship.org/uc/item/0kn8d7pq>

**Author**

Bennett, Anna

**Publication Date**

2022

Peer reviewed|Thesis/dissertation

Improving Pyruvate Kinetic Measurements Using Variable Flip Angle Schemes in bSSFP  
Hyperpolarized Carbon-13 MR Imaging

by  
Anna Bennett

THESIS

Submitted in partial satisfaction of the requirements for degree of  
MASTER OF SCIENCE

in

Biomedical Imaging

in the

GRADUATE DIVISION

of the

UNIVERSITY OF CALIFORNIA, SAN FRANCISCO

Approved:

DocuSigned by:



1644A2CD853841E...

Peder Larson

Chair

DocuSigned by:



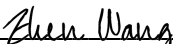
DocuSigned by: 41E...

Daniel Vigneron



DocuSigned by: W45F...

Jeremy Gordon



DocuSigned by: B1BFD...

Zhen Wang

Committee Members



# ACKNOWLEDGMENTS

I would like to thank my advisor, Peder Larson, PhD and my committee members, Daniel Vigneron, PhD, Jeremy Gordon, PhD and Jane Wang, MD for their guidance and support throughout my thesis research. I would also like to acknowledge Xiaoxi Liu, PhD and Charlie Wang, MD, PhD for their contributions in sequence development and flip angle scheme design which were foundational for this work.

Thank you to my family for their love and support and a special thank you to my husband Tim for always encouraging me to pursue my goals.

# Improving Pyruvate Kinetic Measurements Using Variable Flip Angle Schemes in bSSFP Hyperpolarized Carbon-13 MR Imaging

Anna Bennett

## Abstract

Hyperpolarized MR imaging of  $^{13}\text{C}$ -labeled probes provide increased sensitivity to investigate metabolic kinetics. The characterization of  $[1-^{13}\text{C}]$ pyruvate kinetics has been correlated to increased aggressiveness of Renal Cell Carcinoma (RCC) and pyruvate kinetics have the potential to be a valuable tool for assessing disease burden. Increased signal-to-noise ratio (SNR) has already been proven through the use of balanced steady-state free precession (bSSFP) sequences over accelerated gradient echo (GRE) acquisitions. A sigmoid-based variable flip angle scheme was implemented in a pyruvate-specific 3D bSSFP dynamic imaging protocol to further optimize the SNR across multiple acquisitions. The effects of varying flip angle across a dynamic imaging study was first simulated with a physics-based 2-site pyruvate-lactate kinetic model and then evaluated using Monte Carlo simulations for sensitivities to kinetic and imaging parameters. An increase in early lactate signal as well as a delayed pyruvate signal peak and extended signal window were confirmed with subsequent animal studies on a healthy adult rat. The resulting signal changes present the possibility of improved spatial resolution and improved kPL fitting. Additional studies and simulations to optimize associated sequence parameters are needed to further characterize the use-case for sigmoid-based variable flip angle schemes.

# TABLE OF CONTENTS

<b>1</b>	<b>Introduction</b>	<b>1</b>
1.1	Hyperpolarized Signal . . . . .	1
1.2	Carbon-13 Probes & Applications . . . . .	2
1.2.1	[1- <sup>13</sup> C]Pyruvate . . . . .	2
1.3	Sequences . . . . .	3
1.3.1	Variable Flip Angle . . . . .	4
<b>2</b>	<b>Methods</b>	<b>6</b>
2.1	Simulations . . . . .	6
2.2	Animal Studies . . . . .	7
<b>3</b>	<b>Results &amp; Discussion</b>	<b>9</b>
3.1	Simulations . . . . .	9
3.2	Animal Studies . . . . .	12
<b>4</b>	<b>Conclusion</b>	<b>21</b>



# LIST OF FIGURES

1.1	Proposed flip angle evolutions for consecutively acquiring pyruvate and lactate signal. . . . .	5
3.1	Simulated sampled signal of constant flip angle bSSFP acquisition of (a) pyruvate and (b) lactate. . . . .	9
3.2	Simulated, sampled signal of variable flip angle bSSFP acquisition of (a) pyruvate and (b) lactate. . . . .	10
3.3	Simulated sampled signal of constant flip angle GRE acquisition of (a) pyruvate and (b) lactate. . . . .	10
3.4	Simulated, sampled signal of variable flip angle GRE acquisition of (a) pyruvate and (b) lactate. . . . .	11
3.5	Evaluation of accuracy of quantification methods on simulated constant FA GRE data: (a) inputless, fixed $T_1$ of Lactate kinetic model, (b) AUC ratio. The shaded areas represent $\pm 1$ standard deviation while the solid line represents mean fit. . . . .	11
3.6	Evaluation of accuracy of quantification methods on simulated VFA GRE data: (a) inputless, fixed $T_1$ of Lactate kinetic model, (b) AUC ratio. The shaded areas represent $\pm 1$ standard deviation while the solid line represents mean fit. . . . .	12



3.7	Relative error of two different fitting methods on simulated pyruvate and lactate data of a constant FA, GRE acquisition. The dotted lines in each plot represent $\pm 1$ standard deviation. . . . .	13
3.8	Relative error of two different fitting methods on simulated pyruvate and lactate data of a VFA, GRE acquisition. The dotted lines in each plot represent $\pm 1$ standard deviation. . . . .	14
3.9	HP metabolite signal acquired in animal study experiments (a) 1, (b) 2 and (c) 3 (signal has been scaled such that lactate AUC = 1). (d) ROI over center-slice of acquisition from which all signal response data presented are queried. . . . .	15
3.10	Carbon-13 signal acquired in experiment 1. (a) Pyruvate signal overlaid on anatomical images, acquired with VFA bSSFP sequence. (b) Lactate signal overlaid on anatomical images, acquired with constant flip bSSFP. Images represent individual timepoints indicated by the label in the lower left of each pane, temporal resolution: (a) 4.4s, (b) 4.4s. . . . .	17
3.11	Carbon-13 signal acquired in experiment 1. (a) Pyruvate signal overlaid on anatomical images, acquired with constant bSSFP sequence. (b) Lactate signal overlaid on anatomical images, acquired with constant flip bSSFP. Images represent individual timepoints indicated by the label in the lower left of each pane, temporal resolution: (a) 4.4s, (b) 4.4s. . . . .	18
3.12	Carbon-13 signal acquired in experiment 1. (a) Pyruvate signal overlaid on anatomical images, acquired with constant GRE sequence. (b) Lactate signal overlaid on anatomical images, acquired with constant flip bSSFP. Images represent individual timepoints indicated by the label in the lower left of each pane, temporal resolution: (a) 4.7s, (b) 4.8s. . . . .	19

3.13 Alanine carbon-13 signal acquired with constant flip angle GRE sequence. . .	20
---	----

## LIST OF TABLES

2.1	Nominal input parameters for 2-site pyruvate-to-lactate simulations including Monte Carlo (MC) evaluations. . . . .	7
2.2	Sequence parameters utilized for hyperpolarized animal studies. . . . .	8

# 1 Introduction

Carbon is the backbone of many important and complex biological molecules within the human body and therefore plays a role in many biochemical interactions of interest. As an endogenous tracer for magnetic resonance (MR) imaging, it is well positioned to interrogate a broad array of diseases and processes. However, it is not without its limitations. Though carbon is abundant, the natural abundance of the magnetically active  $^{13}\text{C}$  isotope (spin  $\frac{1}{2}$ ) is low ( $\sim 1.1\%$ ). Additionally, the gyromagnetic ratio of  $^{13}\text{C}$  is approximately  $\frac{1}{4}$  that of  $^1\text{H}$ , the natural abundance of which is more than 99%. These differences correspond to a significantly lower sensitivity of  $^{13}\text{C}$  imaging when compared to conventional proton MR [1].

## 1.1 Hyperpolarized Signal

The signal-to-noise ratio (SNR) can be improved by enhancing the relative concentration of  $^{13}\text{C}$  in the imaging probe through isotopic substitution. The nuclear polarization of the resulting  $^{13}\text{C}$ -labeled probe can also be increased by using the technique of dynamic nuclear polarization (DNP). This method of hyperpolarization, or a state of nuclear polarization above that at thermal equilibrium, has been shown to increase signal by more than 10,000-fold, relative to thermal equilibrium [2]. The signal enhancement which hyperpolarization provides is transient and any polarization gained will immediately begin to decay upon dissolution, driven by the  $T_1$  relaxation mechanism. Typical SNR enhancement persists for only 1-2 minutes, consequently rapid imaging techniques are required to minimize loss of signal during image acquisition [3].

## 1.2 Carbon-13 Probes & Applications

Cancer cells rely on metabolic adaptations for biomass production and proliferation [4]. Hyperpolarized  $^{13}\text{C}$  metabolic imaging studies can give indication of staging, treatment response and tumor characterization by imaging evidence of dysregulated metabolic processes in real-time [1, 5]. Hyperpolarized (HP) methods are highly sensitive, detecting only the  $^{13}\text{C}$ -labeled probe and effectively no background signal. To maximize sensitivity, the native substrate selected for the probe should take into consideration the biochemical interactions of the metabolite and the interaction of metabolic pathways with the label site. Site of labeling will also influence the molecule's  $T_1$  relaxation time and therefore affect the rate of hyperpolarized signal decay. The shift in resonant frequency of the  $^{13}\text{C}$  label from native substrate to metabolic product, which also depends on the site of labeling, allows for imaging to isolate the signal source to a specific metabolite. In the case of this study, metabolite-specific excitation pulses are used and pulse profiles are designed to excite either the native substrate or the product but not both. Careful selection of labeling site and design of spectral pulses allows for properly encoded metabolic dynamics. Polarization potential of the labeled probe also is taken into consideration when maximizing available signal.

### 1.2.1 [1- $^{13}\text{C}$ ]Pyruvate

[1- $^{13}\text{C}$ ]Pyruvate is highly relevant for metabolic imaging as it lies at the intersection of several different metabolic pathways. It supports many applications and is well suited for HP studies due to its long  $T_1$  (67s at 3.0T, in solution) and high potential for polarization. It demonstrates adequate chemical shift in downstream metabolites and can be utilized to investigate glycolysis and enzyme activity. After injection, [1- $^{13}\text{C}$ ]pyruvate is metabolized by the enzymes alanine transaminase (ALT) and lactate dehydrogenase (LDH) to [1- $^{13}\text{C}$ ]alanine

and [1-<sup>13</sup>C]lactate respectively [5]. Hyperpolarized imaging of pyruvate-to-lactate conversion is a non-invasive method of measuring this metabolic activity [6].

### 1.3 Sequences

Due to the transient nature of the MR signal of hyperpolarized <sup>13</sup>C-labeled probes, typically GRE sequences are utilized to maximize SNR. Gradient echo sequences support shorter repetition times (TR) which enable rapid 2D and 3D imaging where spin echo sequences are more limited due to the necessary refocusing pulses [7]. Furthermore, the high flip angles required for spin echo sequences can result in rapid loss of the hyperpolarized magnetization. Generally, GRE sequences are comprised of an excitation pulse, gradients and a readout and may include preparation pulses or spoiling. While rapid GRE sequences have been implemented for many studies of hyperpolarized <sup>13</sup>C imaging, more recently the use of balanced steady-state free precession (bSSFP) sequences in imaging [1-<sup>13</sup>C]pyruvate and its downstream metabolites has been studied.

Balanced steady-state free precession sequences have fully balanced gradients, or gradients which over one TR have a net zero area on each axis. In this configuration, the effects of gradients can be ignored in the steady-state condition, and the sequence is characterized by a radio frequency (RF) pulse which alternates in sign each repetition. The transient path of the magnetization will differ depending on initial state of the system but will reach a unique, periodic steady-state based on the RF flip angle. To shorten the transient period, often a catalyzation sequence of RF pulses is used which ramps up to the magnetization steady-state more rapidly. At steady-state, the magnetization is constrained on the surface of an ellipsoid, determined by the  $T_2/T_1$  ratio of the tissue. The signal for a given RF flip angle and precession frequency can then be calculated based on this geometric description. Balanced SSFP sequences are sensitive to off-resonance and signal drop-out can occur when the phase

offset reaches  $\pm\pi$  within the repetition time (TR). Generally, shorter repetition times can avoid banding (signal drop-out) artifacts within the acquisition. As residual transverse magnetization is not spoiled but refocused at the end of the TR, SNR is increased when compared to GRE over dynamic acquisitions.

A metabolite-specific 3D bSSFP (MS-3DSSFP) sequence has been implemented for dynamic  $[1-^{13}\text{C}]$ lactate imaging [8] and  $[^{13}\text{C},^{15}\text{N}_2]$ urea perfusion imaging [9] and demonstrated to improve SNR in comparison to GRE acquisition techniques. Implementation in previous work was performed on a clinical 3T MRI scanner and used a commercial software (RTHawk, HeartVista, Los Altos, CA). The software allows for automated bolus tracking, center frequency calibration and Bloch-Siegert  $B_1$  mapping [6] which occur and are reconstructed in real-time to trigger the acquisition. Implementation of real-time calibrations has demonstrated improvement in consistency and accuracy of imaging results while being an efficient use of non-recoverable magnetization. Variable flip angle schemes were prescribed utilizing this external software.

### 1.3.1 Variable Flip Angle

Variable flip angle schemes have been proposed for dynamic imaging applications as an approach to distribute signal usage evenly throughout the acquisition window or create desired contrast [10, 11]. It has previously been studied in conjunction with bSSFP sequences to optimize cardiac cine imaging, with rapid GRE sequences in optimal HP acquisitions and for the imaging of HP noble gases with bSSFP sequences [12].

The optimal flip angle evolution for encoding the metabolic conversion of  $[1-^{13}\text{C}]$ pyruvate to  $[1-^{13}\text{C}]$ lactate was hypothesized to conform to a sigmoid function (**Figure 1.1**). The use of relatively small flip angles early on in the overall imaging window, aims to preserve longitudinal magnetization for the first several timepoints. This would contribute to a higher

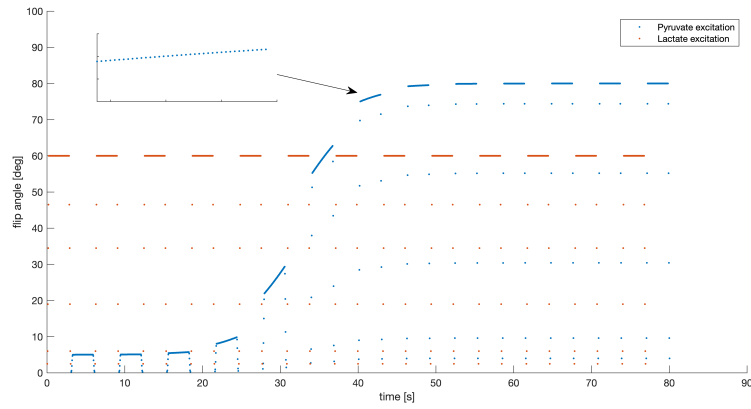


**Figure 1.1:** Proposed flip angle evolutions for consecutively acquiring pyruvate and lactate signal.

initial signal for lactate and a lower initial signal for pyruvate when compared to either GRE or constant flip angle bSSFP acquisitions. Additionally, the scheme shape allows for pyruvate signal to persist over a longer imaging window, possibly allowing for an increase in spatial resolution or the acquisition of additional metabolite products.



## 2 Methods

Support for variable flip angle (VFA) schemes was programmed into an existing pyruvate-specific 3DSSFP sequence designed for acquisition with RTHawk Research software (RTHawk, HeartVista, Los Altos, CA). The RF excitation pulse was scaled in real-time prior to each individual readout to allow for adapting flip angles during a single slab acquisition and across multiple sequence iterations. Variable scaling support was enabled/disabled through the scanner control user interface to ensure that all other parameters of the sequence used remained the same when acquiring with angle variation or with a constant, scalar flip angle value.

Anticipated differences in signal response due to VFA implementation over the use of constant flip angle excitations, was initially characterized with a physics-based simulation and Monte Carlo evaluations. The modified sequence was then tested with a series of hyperpolarized animal studies.

### 2.1 Simulations

An analytical approach based on the Bloch equation, in combination with kinetic modeling formed the basis of simulations performed in MATLAB (The Mathworks Inc., Natick, MA) [13, 14]. Initially, inputless, 2-site pyruvate-to-lactate simulations were performed comparing signal response over 30 timepoints (temporal resolution 3s) during a GRE, constant angle bSSFP and VFA bSSFP acquisition. To further evaluate, a series of Monte Carlo evaluations were run to compare the possible implications of variable flip angle schemes on the perfor-

mance of analysis methods on the quantification of pyruvate-to-lactate conversion. Monte Carlo evaluations are based on a GRE imaging protocol and were defined with parameters that were reasonably equivalent to expected bSSFP characteristics. Parameters for all simulation runs are detailed in **Table 2.1**, estimates for  $T_1$  and  $T_2$  of all metabolites derive from comparable *in vivo* studies [15].

**Table 2.1:** Nominal input parameters for 2-site pyruvate-to-lactate simulations including Monte Carlo (MC) evaluations.

Simulation		Parameters				
bSSFP		$T_1$ [s]	$T_2$ [s]	flip [deg]	$T_{READ}$ [ms]	Timepoints
A	Pyruvate	25	0.6	30	4.2	30
	Lactate		1.3	60	3.8	
B	Pyruvate	25	0.6	VFA	4.2	30
	Lactate		1.3	60	3.8	
MC GRE		$T_1$ [s]	Noise stdev	flip [deg]	TR [s]	Timepoints
C	Pyruvate	25	0.005	15	3	30
	Lactate			30		
D	Pyruvate	25	0.005	0.5*VFA	3	30
	Lactate			30		

## 2.2 Animal Studies

To validate simulated signal responses and confirm functionality of pyruvate specific excitation pulses, animal studies were performed as a part of end-to-end testing. Hyperpolarized

[1-<sup>13</sup>C]pyruvate imaging was performed on a healthy, adult Sprague Dawley rat. The animal underwent 3 identical injections allowing for comparison between GRE, constant flip angle bSSFP and variable flip angle bSSFP acquisitions. All animal experiments were performed according to University of California, San Francisco Institutional Animal Care and Use Committee (IACUC) approved protocols.

Both animal and hyperpolarized [1-<sup>13</sup>C]pyruvate solution preparations were performed as previously reported [8, 9]. Data was acquired with a <sup>1</sup>H/<sup>13</sup>C transceiver single channel birdcage and a minimum of 15 minutes was allowed to elapse between injections. Acquisition parameters for all experiments (injections) are provided in **Table 2.2**.

**Table 2.2:** Sequence parameters utilized for hyperpolarized animal studies.

	Experiment 1	Experiment 2	Experiment 3
Pyruvate	MS 3DSSFP, lactate to pyruvate frequency 385Hz, FOV 8 × 8 × 33.6cm, resolution 2.5 × 2.5 × 21mm, Tread 4.2ms, TR 15.01ms, post acquisition delay 1.55s		MS 2D GRE, FOV 8 × 8 × 21cm, resolution 2.5 × 2.5 × 21mm, Tread 22ms, TR 100ms, flip angle 10°
	variable flip angle	flip angle 30°	
Alanine	N/A		Same as above, alanine to pyruvate frequency -185Hz, flip angle 90°
Lactate	MS 3DSSFP, lactate to pyruvate frequency 385Hz, FOV 8 × 8 × 33.6cm, resolution 2.5 × 2.5 × 21mm, Tread 3.8ms, TR 15.29ms, flip angle 60°		

### 3 Results & Discussion

Results of simulations and animal studies performed to evaluate the execution and effectiveness of variable flip angle acquisitions are presented below as well as discussions on results interpretation and future directions.

#### 3.1 Simulations

Sampled data simulations (presented in terms of SNR) are shown for constant flip angle and variable flip angle in **Figures 3.1** to **3.4**.

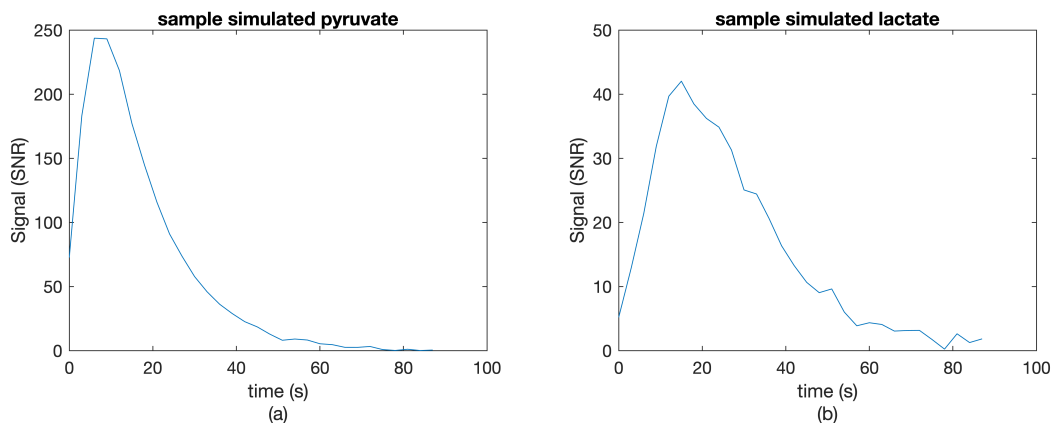


**Figure 3.1:** Simulated sampled signal of constant flip angle bSSFP acquisition of (a) pyruvate and (b) lactate.

Performance of the two analyzed quantification methods (AUC ratio and inputless, fixed  $T_{1,Lactate}$ ) comparing simulated parameters and fitting results for conversion rate have been included in **Figures 3.5** and **3.6**. In **Figures 3.7** and **3.8**, the results of fit sensitivity to various kinetic model input parameters are presented for both methods of quantification.

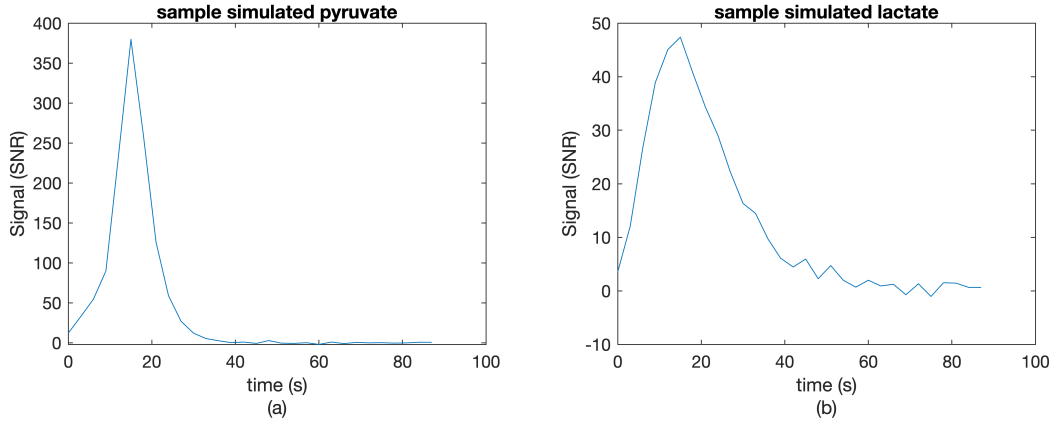


**Figure 3.2:** Simulated, sampled signal of variable flip angle bSSFP acquisition of (a) pyruvate and (b) lactate.

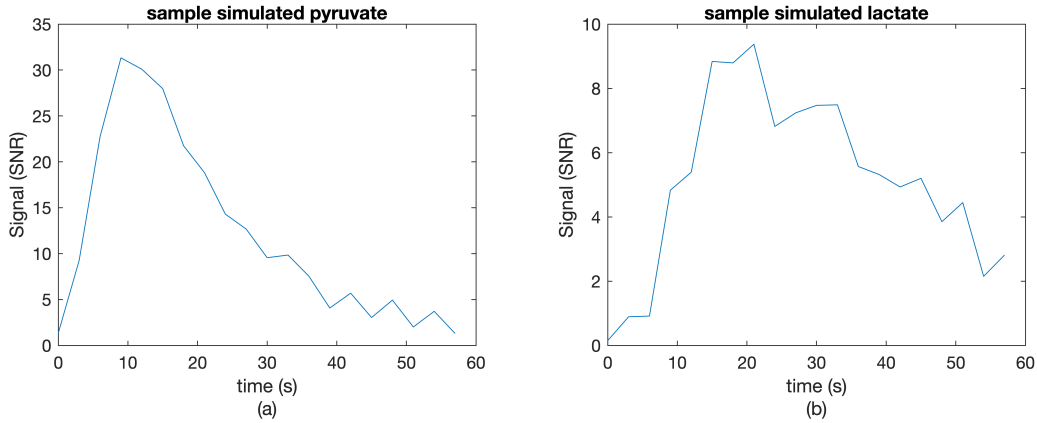


**Figure 3.3:** Simulated sampled signal of constant flip angle GRE acquisition of (a) pyruvate and (b) lactate.

At present, the Monte Carlo evaluation accessible in the *Hyperpolarized MRI Toolbox* [16] is built around a 2-site kinetic model based on the physics of a GRE sequence acquisition of multiple metabolites. Though it is not currently optimized for simulating bSSFP signal responses, we were able to demonstrate relative changes between constant flip angle acquisitions and variable flip angle. When comparing SNR of simulated pyruvate specifically, we note an increase in overall signal and peak signal shifted to a later timepoint in the study. The lactate signal is not appreciably different between the two simulated conditions. These subtle changes in signal, though not a one-for-one representation of potential bSSFP results, can further be utilized to test the performance impact of flip angle selection and optimization

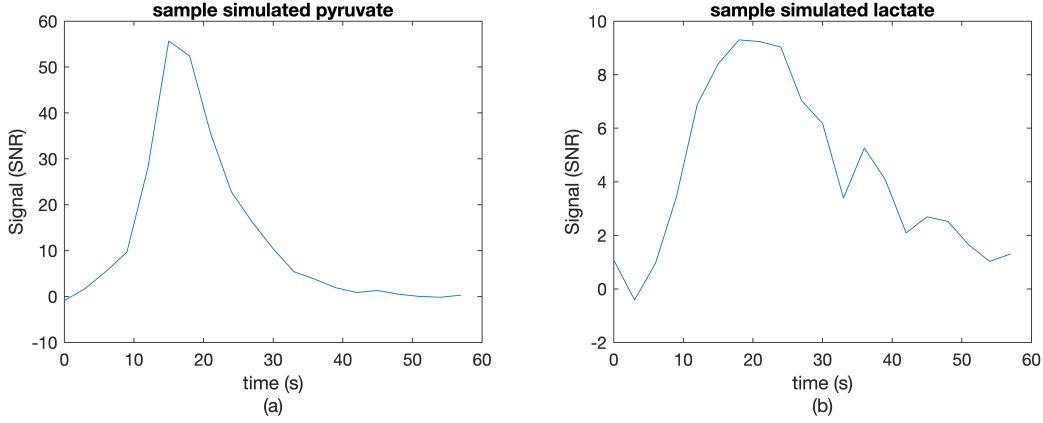


**Figure 3.4:** Simulated, sampled signal of variable flip angle GRE acquisition of (a) pyruvate and (b) lactate.

on different quantification methods.

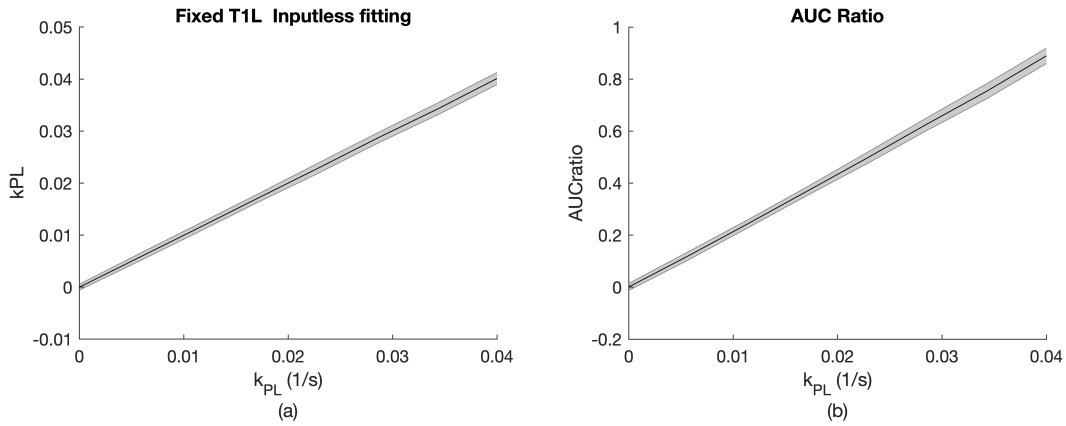


**Figure 3.5:** Evaluation of accuracy of quantification methods on simulated constant FA GRE data: (a) inputless, fixed  $T_1$  of Lactate kinetic model, (b) AUC ratio. The shaded areas represent  $\pm 1$  standard deviation while the solid line represents mean fit.

The two kinetic fitting methods analyzed here (**Figures 3.5** and **3.6**) are consistent between the two simulated conditions. From this we can conclude that the introduction of variable flip angle throughout a dynamic simulation does not introduce a significant bias in fitting when compared to a similar, constant flip angle condition. Sensitivity analyses were run for both constant and variable flip angle conditions on eight separate fitting input parameters. In general, the results show greater variance from the VFA simulated data for both methods and all variables. Also noted in the VFA results, are an increased sensitivity to bolus

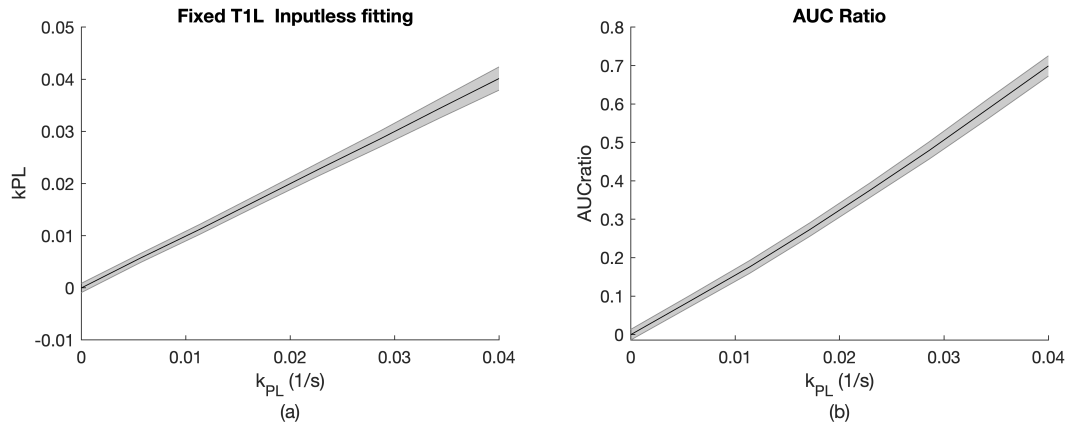


**Figure 3.6:** Evaluation of accuracy of quantification methods on simulated VFA GRE data: (a) inputless, fixed  $T_1$  of Lactate kinetic model, (b) AUC ratio. The shaded areas represent  $\pm 1$  standard deviation while the solid line represents mean fit.

characteristics with AUC ratio fitting and decreased sensitivity to  $B_1$  error also for AUC ratio fitting.

Further work must be done to integrate existing 2-site bSSFP specific kinetic models [14] into the Monte Carlo framework. However, the current results demonstrate the capability of using this evaluation framework to simulate and optimize variable flip angle schemes for GRE sequences and can be extended to include use with bSSFP as well.

## 3.2 Animal Studies

Raw data was acquired from three identical injections on a single day and a single animal. The resulting normalized signal within the subset of slices providing full coverage of both kidneys for each experiment is shown in **Figure 3.9**.

Peak pyruvate signal in the VFA acquisition is shifted to a later timepoint when compared to both constant flip bSSFP and constant flip GRE results. This mirrors simulation results and can possibly explain the higher relative lactate signal in **Figure 3.9a** compared to **Figure 3.9b**. As early pyruvate longitudinal magnetization is preserved and undergoes

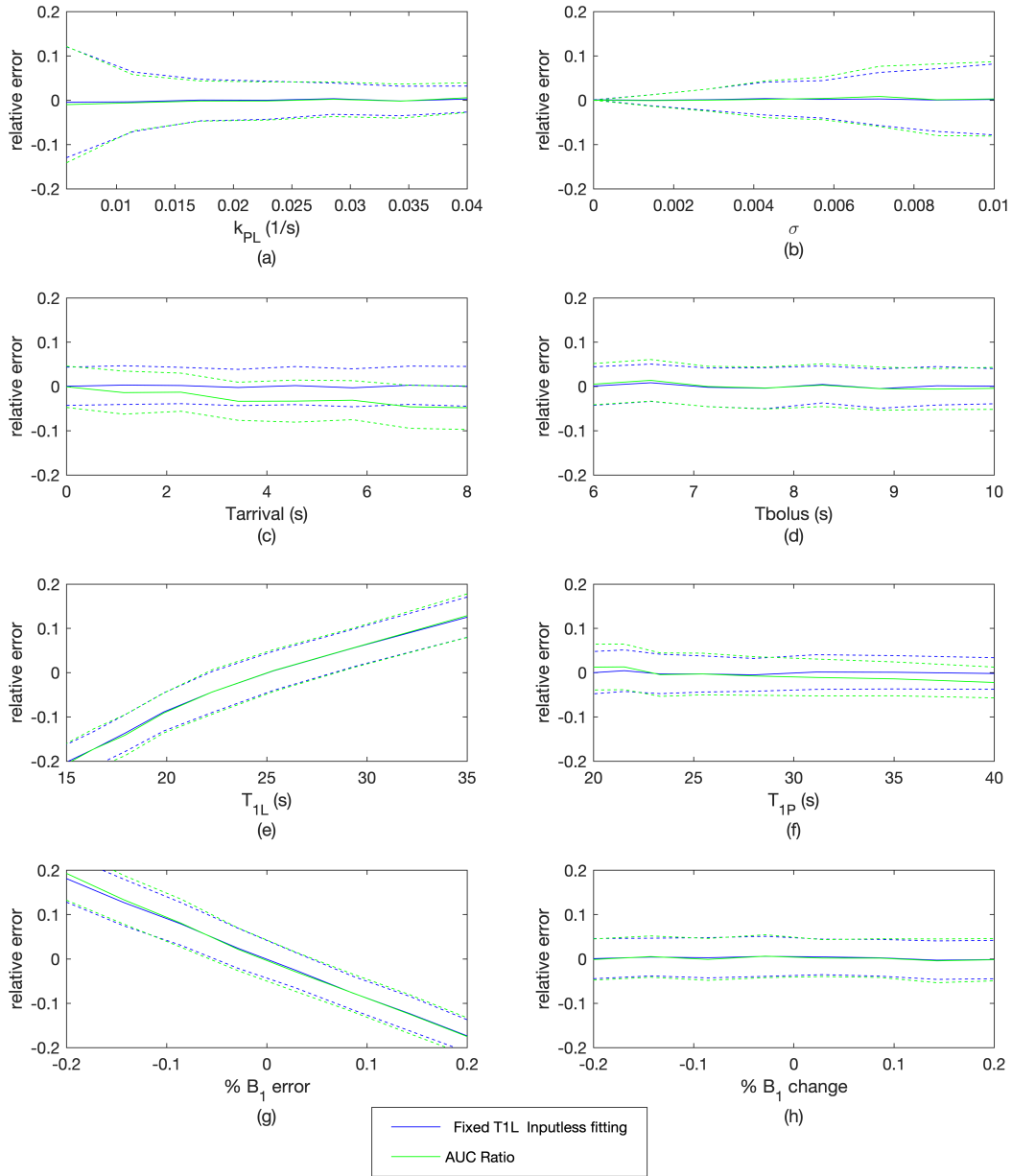


**Figure 3.7:** Relative error of two different fitting methods on simulated pyruvate and lactate data of a constant FA, GRE acquisition. The dotted lines in each plot represent  $\pm 1$  standard deviation.



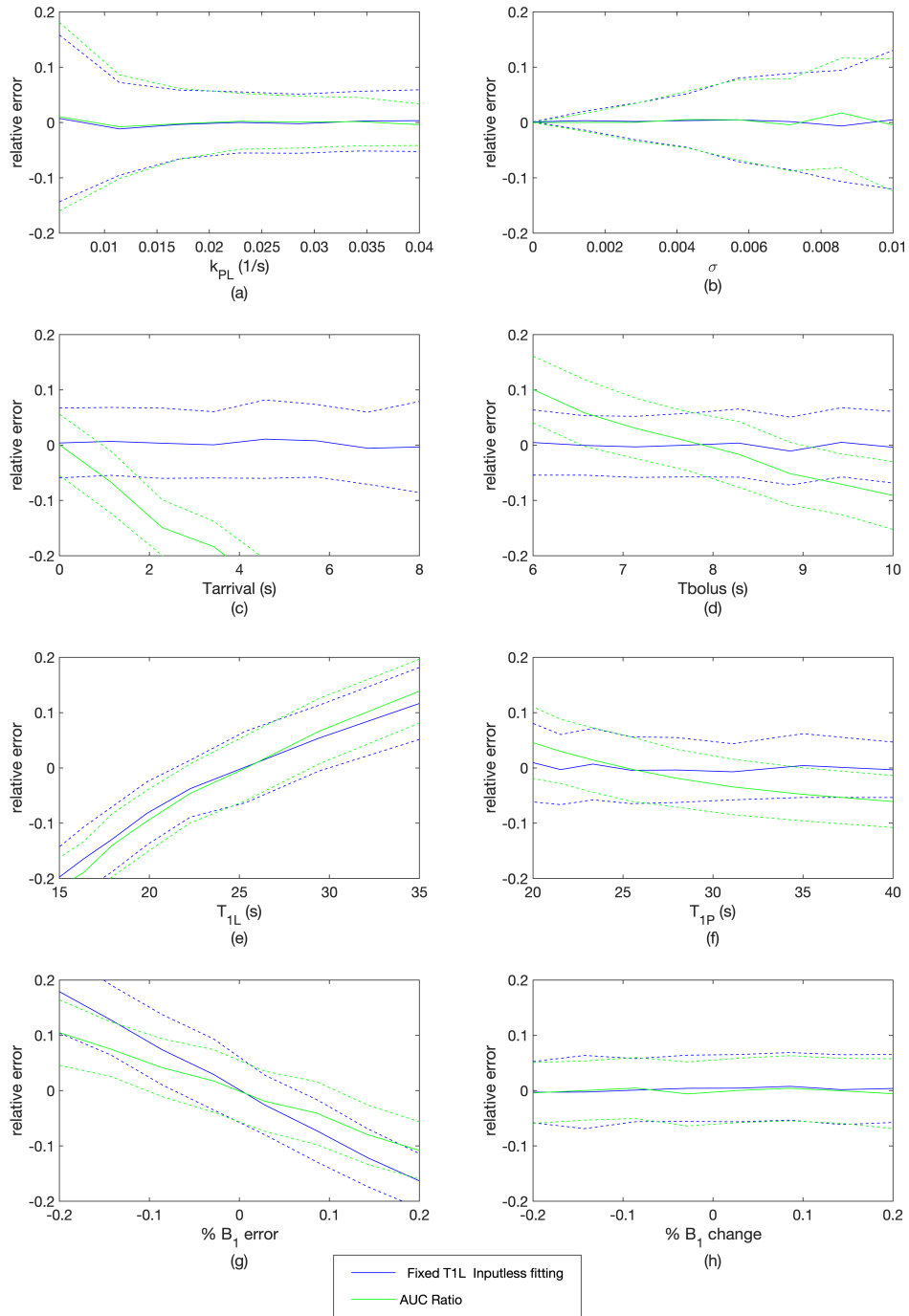
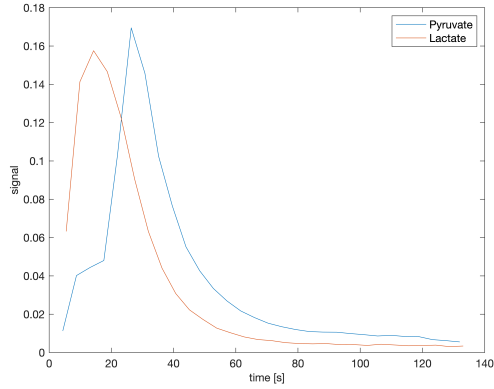
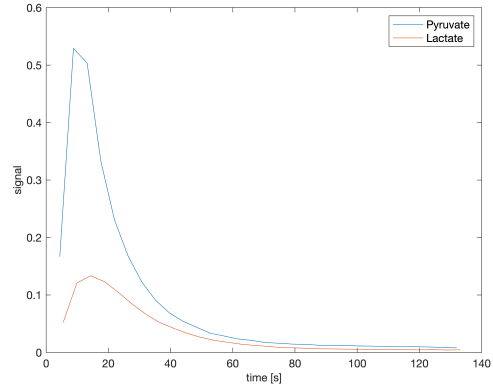


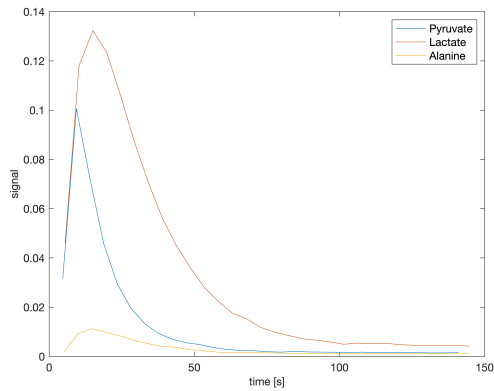
**Figure 3.8:** Relative error of two different fitting methods on simulated pyruvate and lactate data of a VFA, GRE acquisition. The dotted lines in each plot represent  $\pm 1$  standard deviation.



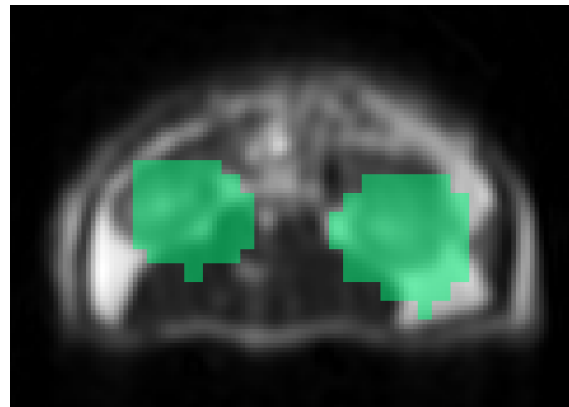
(a) VFA bSSFP



(b) Constant bSSFP



(c) GRE



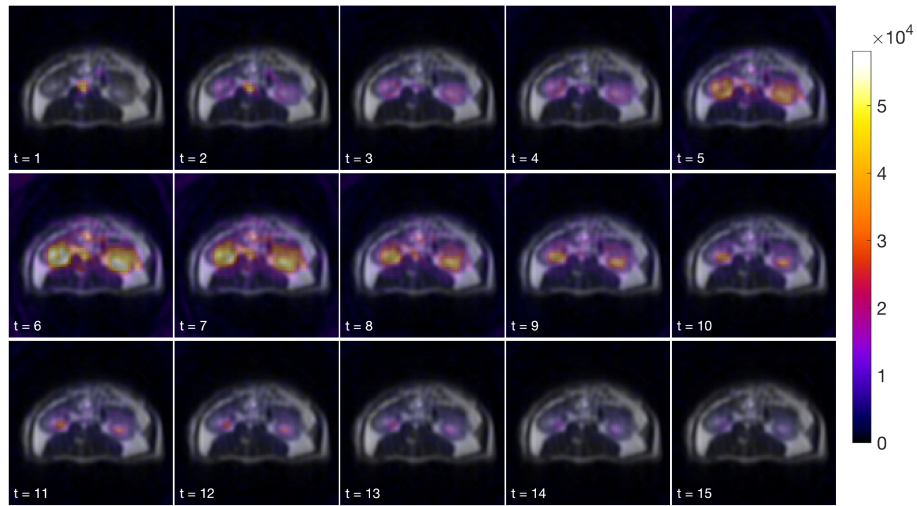
(d) ROI Definition

**Figure 3.9:** HP metabolite signal acquired in animal study experiments (a) 1, (b) 2 and (c) 3 (signal has been scaled such that lactate AUC = 1). (d) ROI over center-slice of acquisition from which all signal response data presented are queried.

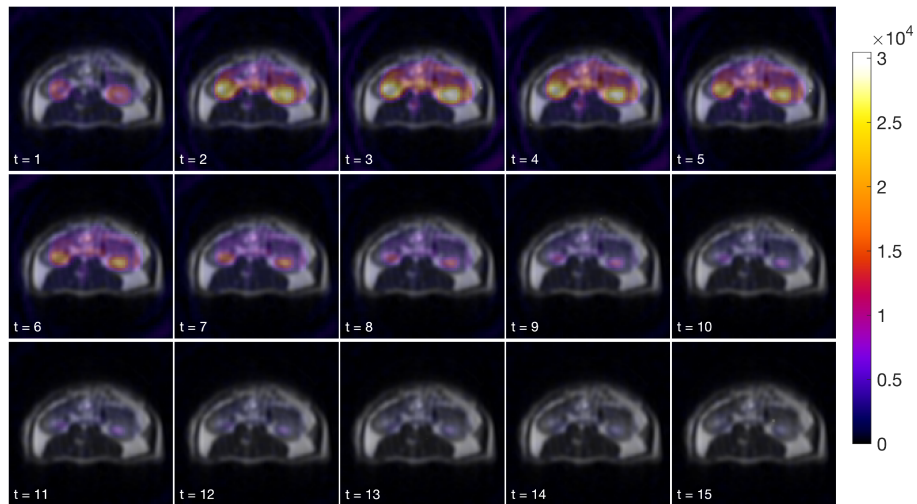
metabolic conversion to lactate we can see increased signal in the lactate acquisition and a well-defined peak. We hypothesize that these features will improve overall kinetic fitting. The GRE results (**Figure 3.9c**) align with previous work demonstrating the increased SNR benefit of bSSFP acquisitions compared to GRE, noted in the overall lower signal of pyruvate compared to lactate. Approximate increase of pyruvate SNR compared to the baseline GRE acquisition was  $1.5\times$  and  $5\times$  for VFA and constant flip angle bSSFP acquisitions respectively.

In **Figures 3.10 to 3.13**, carbon-13 signal has been presented as an overlay on anatomical images collected during the scanning session. A single axial slice at the approximate lateral midpoint of the kidneys was selected to visualize the signal of a single slice collected

iteratively over time. A total of 30 timepoints was collected for each metabolite, in each experiment, however, signal changes are negligible after acquisition 15 and are excluded from these figures for visualization purposes. In experiments 1 and 2, only pyruvate and lactate images were acquired and in experiment 3 alanine was acquired in addition to pyruvate and lactate. As was presented in the signal-time plots above, the variable flip angle experiment pyruvate signal peaks further in the series of acquisitions compared to constant flip angle. Additionally, the pyruvate signal is detected, at low amplitudes, for longer than in experiments 2 or 3. The longevity of pyruvate signal may also contribute to improved kinetic fitting results or allow for finer spatial resolution acquisitions in future studies. Between all three experiments, the lactate acquisition parameters were consistent and the resulting signal maps are consistent in nature as we expected.

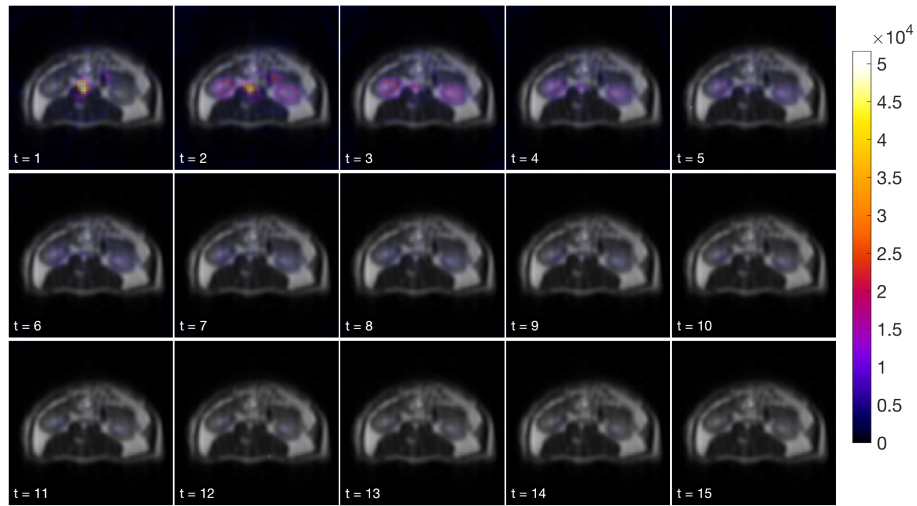


(a) Pyruvate

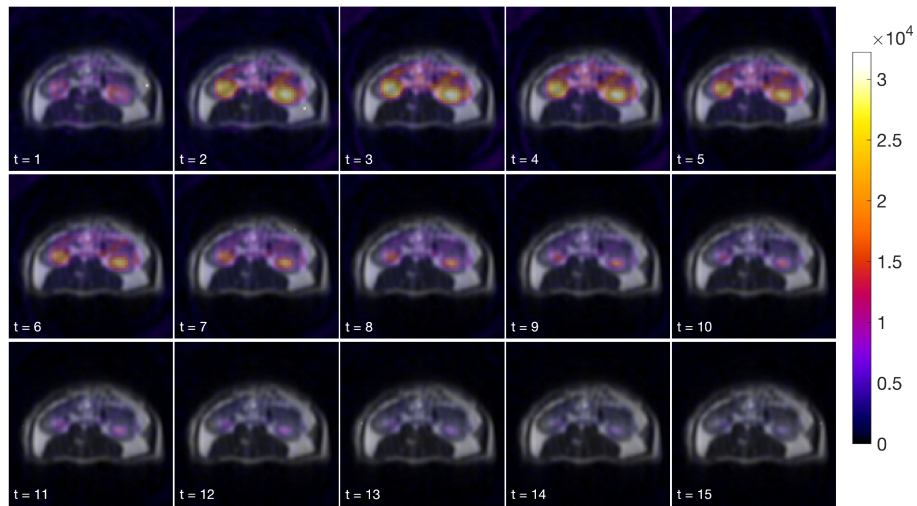


(b) Lactate

**Figure 3.10:** Carbon-13 signal acquired in experiment 1. (a) Pyruvate signal overlaid on anatomical images, acquired with VFA bSSFP sequence. (b) Lactate signal overlaid on anatomical images, acquired with constant flip bSSFP. Images represent individual time-points indicated by the label in the lower left of each pane, temporal resolution: (a) 4.4s, (b) 4.4s.

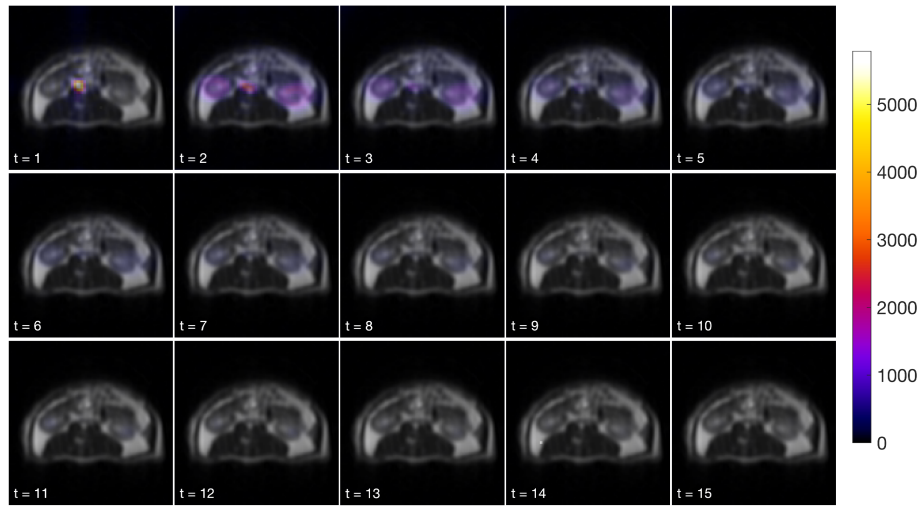


(a) Pyruvate

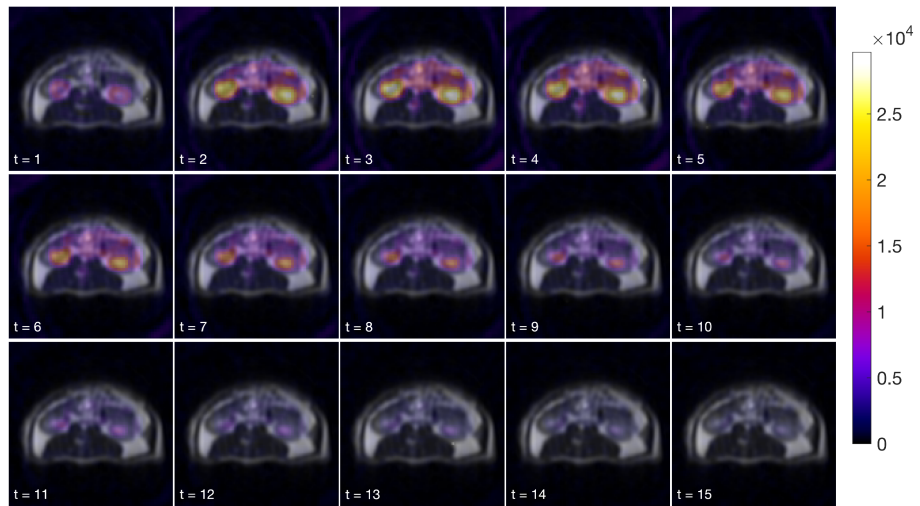


(b) Lactate

**Figure 3.11:** Carbon-13 signal acquired in experiment 1. (a) Pyruvate signal overlaid on anatomical images, acquired with constant bSSFP sequence. (b) Lactate signal overlaid on anatomical images, acquired with constant flip bSSFP. Images represent individual time-points indicated by the label in the lower left of each pane, temporal resolution: (a) 4.4s, (b) 4.4s.



(a) Pyruvate



(b) Lactate

**Figure 3.12:** Carbon-13 signal acquired in experiment 1. (a) Pyruvate signal overlaid on anatomical images, acquired with constant GRE sequence. (b) Lactate signal overlaid on anatomical images, acquired with constant flip bSSFP. Images represent individual time-points indicated by the label in the lower left of each pane, temporal resolution: (a) 4.7s, (b) 4.8s.

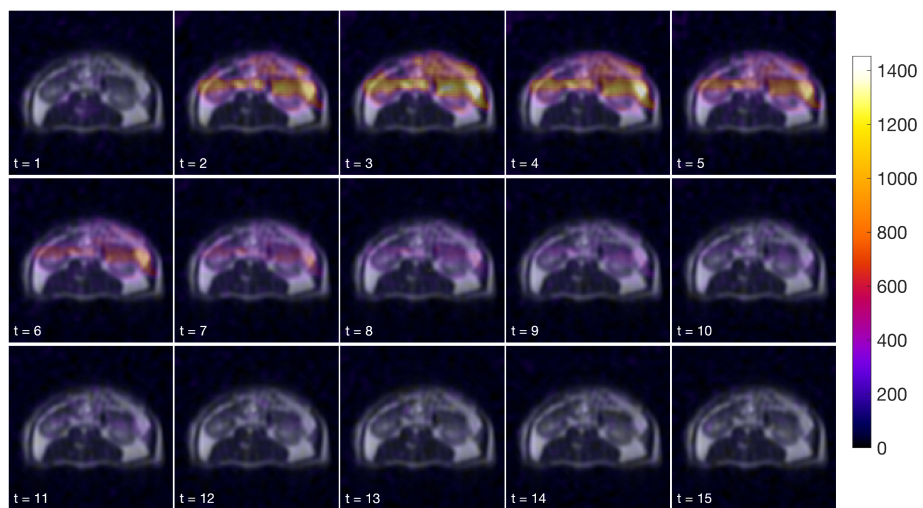


**Figure 3.13:** Alanine carbon-13 signal acquired with constant flip angle GRE sequence.

## 4 Conclusion

Currently, the variable flip angle support feature has been implemented for a  $[1-^{13}\text{C}]$ pyruvate-specific bSSFP sequence and is portable to all metabolite-specific bSSFP sequences defined using the RTHawk software package. Further work is planned to implement a comparative feature in 2D GRE sequence definitions to allow for greater flexibility in experimental protocol design.

Current GRE-based simulation results do not indicate a clear and significant improvement to the fitting methods testing when using variable flip angles, however, simulations have demonstrated that it is a viable framework for future work to implement comparable bSSFP-based simulations and fitting routines. We anticipate the extension of the Monte Carlo evaluation framework to include bSSFP will better predict the performance of a sigmoid-based VFA scheme in use with bSSFP. In addition, relative error analysis results must be extended to include fitting  $T_2$  which is required for adequately supporting bSSFP simulations.

Animal studies were able to demonstrate, at a minimum, the functionality of the sequence programming updates to support VFA. Signal responses of pyruvate experimental data reflected the changes demonstrated in earlier simulation work further confirming the viability of the current VFA implementation and specific flip angle evolution. Additional animal studies will be performed to test alternative schemes, optimize use of signal for improved spatial resolution and test future implementations of the feature for other metabolite-specific bSSFP and GRE sequences.



## References

- [1] Peder E. Z. Larson, I Choi, P Jezzard, Brian Hargreaves, and G Zaharchuk, editors. *HYPERPOLARIZED CARBON-13 MAGNETIC RESONANCE IMAGING AND SPECTROSCOPY*. ELSEVIER ACADEMIC PRESS, S.I., 2021. OCLC: 1220992820.
- [2] Jan H. Ardenkjær-Larsen, Björn Fridlund, Andreas Gram, Georg Hansson, Lennart Hansson, Mathilde H. Lerche, Rolf Servin, Mikkel Thaning, and Klaes Golman. Increase in signal-to-noise ratio of  $> 10,000$  times in liquid-state NMR. *Proceedings of the National Academy of Sciences*, 100(18):10158–10163, September 2003.
- [3] Klaes Golman and J. Stefan Petersson. Metabolic Imaging and Other Applications of Hyperpolarized  $^{13}\text{C}$ . *Academic Radiology*, 13(8):932–942, August 2006.
- [4] Natalya N. Pavlova, Jiajun Zhu, and Craig B. Thompson. The hallmarks of cancer metabolism: Still emerging. *Cell Metabolism*, 34(3):355–377, March 2022.
- [5] Zhen J. Wang, Michael A. Ohliger, Peder E. Z. Larson, Jeremy W. Gordon, Robert A. Bok, James Slater, Javier E. Villanueva-Meyer, Christopher P. Hess, John Kurhanewicz, and Daniel B. Vigneron. Hyperpolarized  $^{13}\text{C}$  MRI: State of the Art and Future Directions. *Radiology*, 291(2):273–284, May 2019.
- [6] Shuyu Tang, Eugene Milshteyn, Galen Reed, Jeremy Gordon, Robert Bok, Xucheng Zhu, Zihan Zhu, Daniel B. Vigneron, and Peder E. Z. Larson. A regional bolus tracking and real-time  $B_1$  calibration method for hyperpolarized  $^{13}\text{C}$  MRI. *Magnetic Resonance in Medicine*, 81(2):839–851, February 2019.

- [7] Brian Hargreaves. Rapid gradient-echo imaging. *Journal of Magnetic Resonance Imaging*, 36(6):1300–1313, December 2012.
- [8] Shuyu Tang, Robert Bok, Hecong Qin, Galen Reed, Mark VanCrickinge, Romelyn Delos Santos, William Overall, Juan Santos, Jeremy Gordon, Zhen Jane Wang, Daniel B. Vigneron, and Peder E. Z. Larson. A metabolite-specific 3D stack-of-spiral bSSFP sequence for improved lactate imaging in hyperpolarized [1-  $^{13}\text{C}$ ]pyruvate studies on a 3T clinical scanner. *Magnetic Resonance in Medicine*, 84(3):1113–1125, September 2020.
- [9] Xiaoxi Liu, Shuyu Tang, Changhua Mu, Hecong Qin, Di Cui, Ying-Chieh Lai, Andrew M. Riselli, Romelyn Delos Santos, Lucas Carvajal, Daniel Gebrezgiabhier, Robert A. Bok, Hsin-Yu Chen, Robert R. Flavell, Jeremy W. Gordon, Daniel B. Vigneron, John Kurhanewicz, and Peder E. Z. Larson. Development of specialized magnetic resonance acquisition techniques for human hyperpolarized [ $^{13}\text{c}$ ,  $^{15}\text{n}_2$ ]urea + [1-  $^{13}\text{c}$ ]pyruvate simultaneous perfusion and metabolic imaging. *Magnetic Resonance in Medicine*, page mrm.29266, May 2022.
- [10] Yan Xing, Galen D. Reed, John M. Pauly, Adam B. Kerr, and Peder E.Z. Larson. Optimal variable flip angle schemes for dynamic acquisition of exchanging hyperpolarized substrates. *Journal of Magnetic Resonance*, 234:75–81, September 2013.
- [11] Kaz Nagashima. Optimum pulse flip angles for multi-scan acquisition of hyperpolarized NMR and MRI. *Journal of Magnetic Resonance*, 190(2):183–188, February 2008.
- [12] Martin H. Deppe and Jim M. Wild. Variable flip angle schedules in bSSFP imaging of hyperpolarized noble gases. *Magnetic Resonance in Medicine*, 67(6):1656–1664, June 2012.
- [13] Peder E. Z. Larson, Hsin-Yu Chen, Jeremy W. Gordon, Natalie Korn, John Maidens, Murat Arcak, Shuyu Tang, Mark Crikinge, Lucas Carvajal, Daniele Mammoli, Robert Bok, Rahul Aggarwal, Marcus Ferrone, James B. Slater, Sarah J. Nelson, John

- Kurhanewicz, and Daniel B. Vigneron. Investigation of analysis methods for hyperpolarized  $^{13}\text{C}$ -pyruvate metabolic MRI in prostate cancer patients. *NMR in Biomedicine*, 31(11), November 2018.
- [14] Sule Sahin, S Tang, M Vaidya, and P Larson. Fitting kinetic rate constants in metabolite-specific bssfp hyperpolarized  $[1-^{13}\text{c}]$ pyruvate mri. In *Virtual Meeting*. International Society of Magnetic Resonance in Medicine, May 2021.
- [15] Eugene Milshteyn, Galen D. Reed, Jeremy W. Gordon, Cornelius von Morze, Peng Cao, Shuyu Tang, Andrew P. Leynes, Peder E.Z. Larson, and Daniel B. Vigneron. Simultaneous T1 and T2 mapping of hyperpolarized  $^{13}\text{C}$  compounds using the bSSFP sequence. *Journal of Magnetic Resonance*, 312:106691, March 2020.
- [16] Jason C. Crane, Jeremy W. Gordon, Hsin-Yu Chen, Adam W. Autry, Yan Li, Maram P. Olson, John Kurhanewicz, Daniel B. Vigneron, Peder E.Z. Larson, and Duan Xu. Hyperpolarized  $^{13}\text{C}$  MRI data acquisition and analysis in prostate and brain at University of California, San Francisco. *NMR in Biomedicine*, 34(5), May 2021.

## Publishing Agreement

It is the policy of the University to encourage open access and broad distribution of all theses, dissertations, and manuscripts. The Graduate Division will facilitate the distribution of UCSF theses, dissertations, and manuscripts to the UCSF Library for open access and distribution. UCSF will make such theses, dissertations, and manuscripts accessible to the public and will take reasonable steps to preserve these works in perpetuity.

I hereby grant the non-exclusive, perpetual right to The Regents of the University of California to reproduce, publicly display, distribute, preserve, and publish copies of my thesis, dissertation, or manuscript in any form or media, now existing or later derived, including access online for teaching, research, and public service purposes.

DocuSigned by:

*Anna Bennett*

3A230D37F43B4A9...

Author Signature

9/1/2022

Date